UAB
Universitat Autònoma de Barcelona

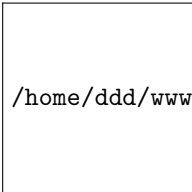**Dipòsit digital de documents de la UAB**

This is the **published version** of the master thesis:

Coello Quihuiri, Edwin Patricio; Abasolo, Ibane , dir.; Corchero Nieto, José Luis. Optimization of Enzyme Replacement Therapy Using Vesicles as Delivery Vehicles for alpha galactosidase (GLA) for the treatment of Fabry disease. 2025. 32 pag. (Màster Universitari en Bioquímica, Biologia Molecular i Biomedicina)

This version is available at https://ddd.uab.cat/record/320209

/home/ddd/www/img/licenses/zero.jpg

under the terms of the license

Autonomous University of Barcelona

Optimization of Enzyme Replacement Therapy Using Vesicles as Delivery Vehicles for alpha galactosidase (GLA) for the treatment of Fabry disease.

Edwin Patricio Coello Quihuiri

Master Thesis
Master's Degree in Biochemistry, Molecular Biology, and Biomedicine with a specialization in Molecular Pathology

Supervisors

Dra. Ibane Abasolo

Dr. José Luis Corchero Nieto

2025

Edwin Patricio Coello Quihuiri

Dr. José Luis Corchero Nieto   Dra. Ibane Abasolo

Index

Summary

In the first part of the project, production of α-galactosidase A (GLA) was carried out using two strategies: transient transfection in HEK293F cells and expression in a stable clone of CHO cells. Three variants were obtained: HEK GLA-HIS, HEK GLA cmyc, and CHO GLA CMYC. The highest expression was observed in CHO GLA CMYC, in line with previous reports highlighting CHO cells for their high efficiency and stability in recombinant protein production. The HEK GLA CMYC variant outperformed HEK GLA HIS, potentially due to the stabilizing effect of the CMYC tag. In contrast, the HIS tag may negatively affect the solubility and functionality of GLA., Soluble, secreted GLA was purified by affinity chromatography with His SpinTrap columns. Exposure to imidazole and high pH during purification steps reduced enzymatic activity, necessitating a subsequent dialysis step.

The second phase of the project focused on the purification of extracellular vesicles (EVs) loaded with GLA, using two methods: bottom-through filtration (BTF) and tangential flow filtration (TFF). TFF outperformed BTF in terms of yield and preservation of enzymatic activity, due to its gentler flow conditions. CHO GLA CMYC cells not only produced a higher quantity of EVs but also generated vesicles with enhanced enzymatic activity. This is attributed to the superior folding capacity and post-translational modification machinery of CHO cells. The CHO GLA CMYC system, combined with TFF purification, emerges as an efficient and scalable platform for the development of an extracellular vesicle-based enzyme replacement therapy (ERT) for Fabry disease.

Abbreviation List

4-MU
  4-methylumbelliferone

A

A (GLA).
  alpha galactosidase
ADAs
  neutralizing antibodies

B

BBB
  blood brain barrier

Ch

CHO
  Chinese hamnster ovary

D

DDS
  drug delivery systems

E

EPR
  enhanced permeability and retention
ER
  endoplasmic reticulum
ERT
  enzyme renplacement therapy
EVs
  extracellular vesicles

F

FD
  Fabry disease

G

Gb3
  globotriaosylceramide

H

HEK293

L

LSDs
  lysosomal storge disorders

M

M6P
  mannose-6-phosphate
M6PR
  mannose-6-phosphate receptor
MSCs
  mesenchymal stem cells
MVs
  micro vesicles

P

PBS
  phosfate buffer saline
PC
  pellets cells
PEG
  polyethylene glycol
PTA
  phosphotungstic acid

S

SNs
  supernatants

1. Introduction

1.1. Fabry disease

Fabry disease is one of the most common lysosomal storage disorders (LSDs) and is caused by a genetic mutation in the *GLA* gene, located on the X chromosome at position Xq22.1. This mutation leads to a deficiency or complete absence of the lysosomal enzyme α-galactosidase A (GLA) as shown in the schematic in Figure 1. The disorder affects both males and females, and its prevalence varies widely, with estimates ranging from 1 in 40,000 to 1 in 120,000 live births (Miller et al., 2020; West et al., 2009).
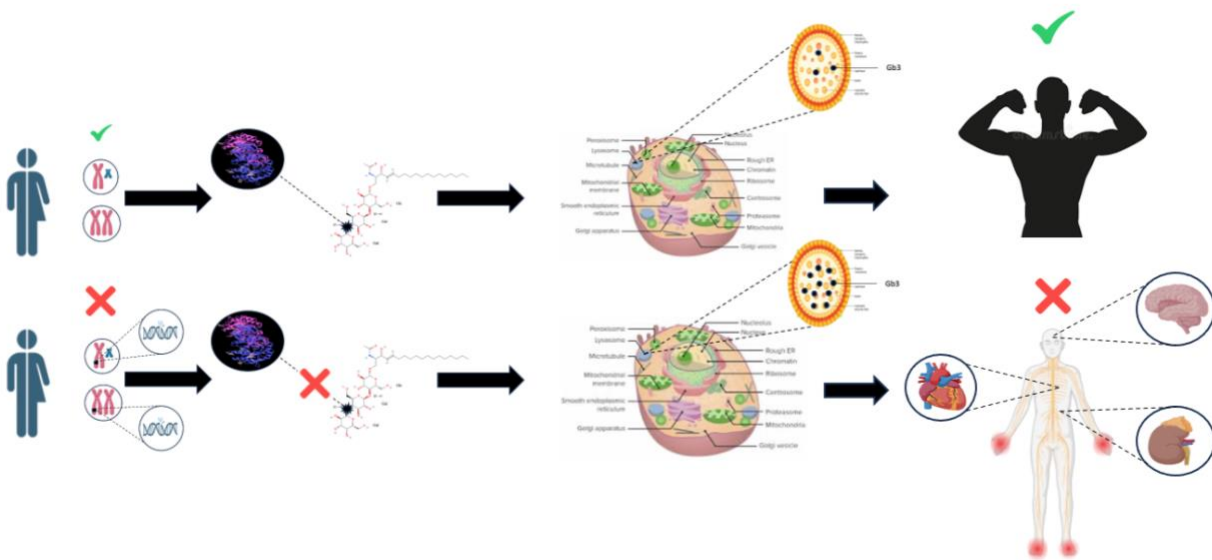

Figure 1. Damage to the GLA gene results in partial or complete deficiency of α-galactosidase A, leading to the accumulation of Gb3.

The deficiency in GLA activity leads to a progressive accumulation of neutral glycosphingolipids, particularly globotriaosylceramide (Gb3), within the lysosomes of various cell types (Guérard et al., 2017). Gb3, composed of a ceramide linked to a sugar chain (one glucose and two galactose residues), is the primary substrate normally degraded by the GLA enzyme. When not properly eliminated, this lipid accumulates mainly in endothelial, cardiac, renal, and neuronal cells, impairing their normal function. (Hughes et al., 2023).
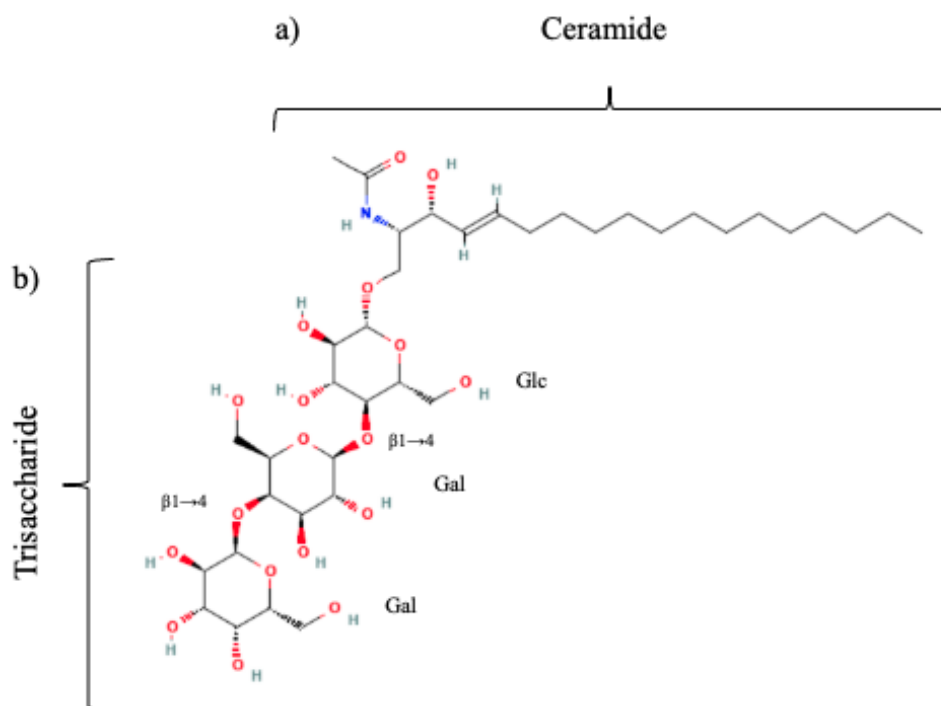
Figure 2. Globotriaosylceramide (Gb3). a) Composed of two main parts: Ceramide (a sphingosine lipid base and a fatty acid linked by an amide bond), b) Trisaccharide (one glucose and two galactose units). Image modified from PubChem/NCBI, 2015.

Vascular endothelial cells are particularly sensitive to this accumulation, which interferes with essential cellular processes such as metabolism, redox balance, and ion transport through membrane channels. This cellular dysfunction leads to a variety of multisystemic clinical manifestations (Alipourfetrati et al., 2015).

Early symptoms usually appear during childhood or adolescence and include skin lesions angiokeratomas, gastrointestinal discomfort, and neuropathic pain. As the disease progresses into adulthood, more severe complications may develop, such as cardiomyopathies, renal failure, and cerebrovascular events including ischemic strokes or hemorrhages. In the absence of treatment, disease progression can lead to multiorgan deterioration and premature death (Azevedo et al., 2020).

1.2. GLA

α-galactosidase A (GLA) is a glycosylated lysosomal hydrolase enzyme composed of 429 amino acids. Its synthesis begins in the endoplasmic reticulum (ER), where it is produced as

a preprotein containing a signal peptide. Its molecular weight is approximately 50 kDa. (Abasolo et al., 2021; Ferreira & Gahl, 2017). This signal peptide is cleaved during enzyme maturation, producing an active form with a lower molecular weight between 46 and 51 kDa. After synthesis in the ER, the enzyme undergoes modifications in the Golgi apparatus, where its N-linked oligosaccharide chains receive mannose-6-phosphate (M6P) groups. These modifications are essential for recognition by M6P receptors and for targeting the enzyme to the lysosome (Coutinho et al., 2016; Ferreira & Gahl, 2017).

Under normal conditions, mature GLA is located in the lysosome as a homodimer composed of two identical subunits. Each subunit contains two structural domains: an N-terminal domain (residues 32–330), which adopts a $(\beta/\alpha)_8$ barrel fold and contains the active site, and a C-terminal domain (residues 331–429) with an antiparallel β-sheet structure. Each enzyme subunit has three N-glycosylation sites, with residue N215 being particularly critical, as it significantly contributes to the solubility, stability, and correct intracellular trafficking of the enzyme from the ER to the lysosomes.

During this process, a fraction of the enzyme can be secreted into the extracellular space and taken up by nearby cells through mannose-6-phosphate (M6P) receptor-mediated endocytosis at the plasma membrane, allowing its re-entry into lysosomes.
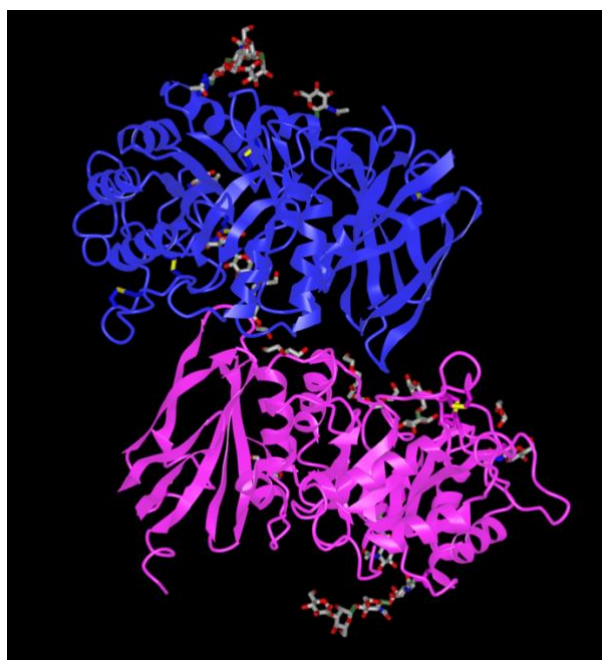

Figure 3. Human alpha – galactosidase is composed of two identical monomers, shown in different colors, forming a homodimer. NCB (2025).

1.3. Treatment

The standard treatment for Fabry disease since 2001 has been enzyme replacement therapy (ERT), in which α-galactosidase is administered parenterally to reduce globotriaosylceramide (Gb3) levels in blood and tissues. This leads to a decrease in neuropathic pain, gastrointestinal problems, and progressive organ deterioration. Although relatively effective, the treatment cannot reverse or cure the disease (Alipourfetrati et al., 2015; Hughes et al., 2023).

Among the approved drugs for the treatment of Fabry disease (FD), there are three main options: Replagal®, which is agalsidase alfa produced in human fibroblasts and administered as a liquid formulation at a dose of 0.2 mg/kg; Fabrazyme®, which is agalsidase beta produced in Chinese hamster ovary (CHO) cells, administered at 1 mg/kg in a lyophilized form; and **Elelyso®** (Elfabrio®), which is pegunigalsidase alfa produced using a plant-based system derived from tobacco called ProCellEX®. Its main characteristic is polyethylene glycol (PEG) modification, providing increased stability and longer half-life. It is administered at 1 mg/kg. In all cases, regardless of the drug used, treatment is given every 15 days.(Alipourfetrati et al., 2015; Hughes et al., 2023).

Both agalsidase alfa and beta are recombinant forms of the human GLA enzyme, thus sharing similar biochemical characteristics. However, there are slight differences in their glycosylation patterns and in their uptake mechanisms mediated by the mannose-6-phosphate receptor (M6PR).

Among the limitations of these drugs are their inability to cross the blood-brain barrier (BBB), low enzymatic stability and rapid degradation, limited biodistribution, the requirement for recurrent intravenous infusions, potential formation of neutralizing antibodies (ADAs), and high immunogenicity. Additionally, the high cost of these treatments can exceed €280,000 per patient (Morimoto et al., 2018; Nakamura et al., 2020; Wallace et al., 2024).

1.4. Nanomedicine

Nanomedicine is a branch of medicine that applies various tools from nanotechnology for the treatment, diagnosis, and monitoring of diseases. Regarding treatment, nanotechnology has become a powerful tool as it can deliver drugs in a targeted and precise manner, making

it useful in combination with traditional therapies through drug delivery systems (DDS) (Zeb et al., 2020). It consists of a drug encapsulated within a nanocarrier that transports it to the specific site of action. Among the benefits of this method are the reduction of toxicity associated with traditional drugs, protection of the drug from degradation thereby increasing its half-life, and improved solubility. (Wilczewska et al., 2012)

Due to their low oral absorption, DDS are usually administered intravenously. Once in the bloodstream, the nanoparticles utilize their targeting mechanism, which can be passive or active. Passive targeting occurs when DDS accumulate in vascularized tissues at pathological sites through the enhanced permeability and retention (EPR) effect. Inflamed tissues surrounding tumors tend to be more permeable, allowing small nanoparticles of approximately 150 nm to cross the blood vessel walls and accumulate at the target site (Juszkiewicz et al., 2020; Yetisgin et al., 2020), In contrast, active targeting relies on the binding of specific molecules such as peptides, antibodies, or nucleic acids to the surface of the nanoparticle, allowing for enhanced uptake of the DDS in the tissues of interest. The elimination of DDS occurs primarily through the reticuloendothelial system (RES), which is present in the liver, spleen, lungs, and bone marrow (Bozzuto & Molinari, 2015; Glassman & Muzykantov, 2019; Torchilin, 2005), Macrophages recognize and eliminate DDS, and opsonization facilitates this removal through serum proteins, such as antibodies, which adsorb onto the surface of the nanoparticles (NP), promoting their clearance (Glassman & Muzykantov, 2019)

There is a wide variety of nanocarriers as potential vehicles for drugs, depending on their size, surface functionality, and the nature of the nanoparticle. In the specific case of Fabry disease, the goal is to improve enzyme replacement therapy by protecting the enzyme from degradation, reducing its immunogenic response, and increasing penetration across the blood-brain barrier (BBB) (Abasolo et al., 2021; Del Grosso et al., 2022; Lu et al., 2022; Seras-Franzoso et al., 2021).

1.5. Extracelular Vesicles (EVs)

They are small membrane-bound structures that can be classified according to their origin into extracellular vesicles (EVs): exosomes, ranging from 30 to 150 nm; microvesicles (MVs), from 100 to 1000 nm; and apoptotic bodies, from 1 to 5 μm. These vesicles can carry

a wide variety of molecules such as proteins, lipids, and nucleic acids, thus acting as vehicles for intercellular communication and influencing various biological processes (Doyle & Wang, 2019). The biogenesis of exosomes occurs via the endocytic pathway, involving the invagination of the plasma membrane to form early endosomes (Leone et al., 2018; Ståhl et al., 2019). The natural content of EVs is determined by the cell type from which they originate and the mechanisms involved in their formation. EVs can be classified into two main groups: natural EVs, which have not been modified and are produced by the cells themselves with therapeutic properties. An example of this is mesenchymal stem cells (MSCs), which show potential for tissue repair due to their ability to home to sites of inflammation and modulate the immune response (Abreu et al., 2020; Sahoo et al., 2021). Modified EVs are engineered to carry bioactive molecules. This is achieved through genetic alterations in the producing cells to increase the expression of the protein of interest. Additionally, ligands can be used to target these EVs to specific cells or tissues, thereby enhancing their therapeutic impact (Cooper et al., 2014; Gupta et al., 2021). The biodistribution and clearance of EVs is rapid, with an initial half-life of approximately 20 minutes followed by a secondary half-life of around 180 minutes. Clearance is primarily mediated by phagocytes, with total elimination times ranging between 6 and 48 hours depending on the type of EVs. Regarding their distribution, within the first 30 minutes post-administration, the majority of EVs accumulate in the liver, followed by smaller amounts in the spleen, kidneys, and lungs (Lenders et al., 2020; Rombach et al., 2012).

Among the drawbacks of EVs as a therapy is their variability, which directly affects size, surface marker content, characterization, and dosing, posing a challenge for standardizing their production (Kimiz-Gebologlu & Oncel, 2022). Another important drawback is targeting specificity, as EV uptake should occur only in the target tissue. Additionally, modifying the surface of EVs may trigger an immune response.

ERT for Fabry disease faces several limitations, including the short half-life of the administered enzyme, variability in production efficiency, and the potential to elicit immune responses. To address these issues, the use of extracellular vesicles (EVs) derived from HEK and CHO cells as delivery systems for α-galactosidase A (GLA) represents a promising alternative. EVs may offer protective encapsulation of the enzyme, enhancing its stability in circulation, reducing immunogenicity, and improving cellular uptake. Furthermore,

optimizing EV production through the use of stable cell lines and robust purification protocols could mitigate batch-to-batch variability and enhance therapeutic consistency. These improvements are essential to increase the efficacy and safety profile of ERT and support its translation into more reliable and scalable clinical applications. Hypothesis

The therapeutic efficacy of extracellular vesicles loaded with α-galactosidase A depends on the producer cell line (HEK293 or CHO) and the isolation method, which influence the yield, enzymatic activity, and quality of the vesicles.

Objectives

1.6. General Objective

To evaluate how the producer cell line HEK293F or CHO and the isolation method affect the production, quality, and enzymatic activity of extracellular vesicles (EVs) loaded with α-galactosidase A (GLA) for their potential use in enzyme replacement therapy for Fabry disease.

1.7. Specific Objectives

- To compare the yield and quality of EVs produced by HEK293F and CHO cell lines expressing α GLA.

- To analyze the impact of different isolation methods on the purity, integrity, and enzymatic activity of EVs loaded with GLA.

- To assess the functional enzymatic activity of the obtained EVs to determine their therapeutic potential.

- To identify optimal production and purification conditions to maximize the efficacy of EVs as a delivery system for Fabry disease therapy.

2. Materials and Methods

2.1. Plasmids production

The plasmids used for transfections were pOpinE-GLA, pTRIX1.1-GLA-cMyc-His2, and pAdVantage. For their preservation and amplification, competent *Escherichia coli* DH5α cells were used. These cells were thawed at 4 °C for approximately 30 min to maintain their viability. Once completely thawed, 5 µL of the corresponding plasmid was added to 50 µL of competent cells under sterile conditions inside a biosafety cabinet. The mixture was incubated on ice for 30 min.

Subsequently, a heat shock was performed at 42 °C for 45 s to facilitate the uptake of the plasmid by the bacterial cells, after which the mixture was returned to ice for two minutes. Meanwhile, 950 µL of pre-warmed SOC medium was added to the transformed cells to initiate the recovery phase. This mixture was incubated at 37 °C with constant shaking for one hour.

After recovery, 100 µL of the culture was plated onto LB agar plates supplemented with ampicillin (100 µg/mL), which were incubated at 37 °C overnight. The following day, colonies with morphological characteristics consistent with successful transformants were selected and inoculated into 500 mL of liquid LB medium containing ampicillin and cultured under constant shaking at 37 °C overnight for further analysis and preservation.

The culture was then centrifuged, and plasmid DNA was extracted using the commercial PureLink™ HiPure Plasmid Giga Kit (Invitrogen™) protocol. The concentration and purity of the obtained plasmid DNA were determined by spectrophotometry, using the A260/A280 ratio as an indicator of purity. Values between 1.8 and 2.0 were considered acceptable. The obtained DNA was aliquoted and stored at -20 °C until use in transfections.

2.2. Production of GLA-HIS and GLA-Cmyc

For the transient production of GLA-His and GLA-cMyc-His, the HEK293F cell line adapted to suspension culture was used. Cells were maintained under continuous agitation in Erlenmeyer flasks in serum-free medium, specifically FreeStyle™ 293 Expression Medium (ThermoFisher), at 37 °C, 8% CO_2, and 125 rpm in a shaking incubator. The culture was divided into three 250 mL flasks each (triplicates), labeled n1, n2, and n3 for GLA-His and

another three flasks labeled n1, n2, and n3 for GLA-cMyc-His. The cell density at the time of transfection was adjusted to 1.06×10^6 cells/mL.

For the transient transfection of GLA-His, the plasmid pOpinE-GLA at a concentration of 0.99 µg/µL was used. The total volume to transfect was 750 mL with 0.5 µg pDNA/mL, therefore 375 µg of pDNA was used, equivalent to 379 µL of plasmid. Additionally, the plasmid pAdVantage at 0.88 µg/µL was used, with the same transfection volume and 0.2 µg pDNA/mL, resulting in 150 µL of plasmid and 1575 µL of PEI as the transfection agent in a 1:3 (DNA:PEI, weight/weight) ratio.

For the transient transfection of GLA-cMyc-His, two plasmids were used: pTriEx1.1-GLA-cMyc-His at 1.08 µg/µL concentration, with a transfection volume of 750 mL and 0.5 µg pDNA/mL, resulting in 170 µL of pDNA. The second plasmid was pAdVantage at 0.88 µg/µL with the same volume and 0.2 µg pDNA/mL, resulting in 170 µL of pDNA and 1575 µL of PEI in a 1:3 (DNA:PEI, weight/weight) ratio.

For both GLA-His and GLA-cMyc-His transfections, the above-described mixtures were prepared in 250 mL flasks with 75 mL of medium. The mixtures were vigorously vortexed for 30 s and incubated at rest for 10 min. Subsequently, 25 mL of the mixture was dispensed into each Erlenmeyer flask, which were then incubated at 37 °C, 8% CO_2, and 130 rpm. Approximately 20 h after transfection, VPA was added to a final concentration of 4 mM, from a stock at 500 mM.. Five days later, cultures were collected and cell counts performed. Cultures were centrifuged for 10 min at 5000 rpm to obtain supernatants (SNs). The SNs were separated, and the cell pellet (PC) was resuspended in PBS and stored at -20 °C.

2.3. Clone stable CHO

A stable clone for the production of GLA-cMyc-His in CHO cells was used, cultured in CD-CHO basal medium without the GS supplement. This clone had been previously originated at IBB – UAB. Three cryovials were thawed and cultured separately to maintain variability between triplicates. Cell counting and dilutions were performed for subsequent expansion. Cultures were collected and centrifuged for 15 minutes at 5000 rpm to obtain supernatants (SNs) and cell pellets (PC), which were resuspended in PBS and stored at -20 °C.

2.4. Purification of GLA soluble

Three replicates were processed, each composed of n1 (HIS1, CMYC1, CHO1, and CONTROL 1), n2 (HIS2, CMYC2, CHO2, and CONTROL 2), and n3 (HIS3, CMYC3, CHO3, and CONTROL 3). His SpinTrap columns (Cytiva®) were used for purification using th vendor protocol and instructions, .

Once equilibrated, 600 µL of sample (clarified SN) was added to the columns, followed by centrifugation at 100 × g for 30 s. The eluate was discarded, and another 600 µL of sample was added and centrifuged again under the same conditions. A wash step was performed by adding 600 µL of binding buffer and centrifuging at 100 × g for 30 s. The collection tube was replaced, and 200 µL of elution buffer was added, followed by centrifugation at 100 × g for 30 s. This elution step was repeated once more with an additional 200 µL of elution buffer and centrifugation under the same conditions.

Approximately 400 µL of protein in elution buffer was collected, and all samples were adjusted to a final volume of 1.5 mL by adding 1.1 mL of cold PBS. The samples were then subjected to dialysis using a buffer exchange cassette. 1.5 mL of sample was placed into each cassette, sealed, and immersed in a beaker containing 300 mL of cold PBS under constant agitation. The PBS was changed every 15 min for a total of 1 hour. The dialyzed samples were collected in 2 mL Eppendorf tubes, yielding approximately 1.5 mL per sample, and stored at -20 °C.

2.5. Quantification Western Blot WB

To detect and quantify the recombinant proteins, SDS-PAGE was performed by using TGX Stain-Free™ FastCast™ acrylamide at 12% (Bio-Rad, ref. 161-0185), and further visualization of proteins with a ChemiDoc™ Touch Imaging System (Bio-Rad). In some cases, further western-blot analyses were performed. To detect the different GLA mutants, an anti-GLA rabbit polyclonal antibody (Merck, ref. HPA000237), or anti-His mouse monoclonal antibody (Clontech, ref. 631212), were used as primary antibodies. Amounts of GLA enzymes were densitometrically estimated by comparison, after SDS-PAGE and western-blot analyses, with known amounts of a control His-tagged GLA produced and purified in-house and quantified by the BCA method. Samples and standards to be

quantitatively compared were run in the same gel and processed as a set. Densitometric analyses of the immunoreactive bands were performed with the Image Lab™ software (version 5.2.1., Bio-Rad).

2.6. Purification de EVs BTF y TFF

2.6.1. Bentochtop filtration (BTF)

A centrifugation was started at 10,000 × g for 30 min at 4 °C for each sample n1, n2, and n3, respectively. To concentrate the EVs, free proteins were removed using Centricon Plus-70 filters with a 100 kDa cutoff. The supernatant was centrifuged in the Centricons at 3,500 × g for 20 min at 4 °C, and the filtrate was discarded. These steps were repeated as many times as necessary until the entire supernatant had passed through the filter.

Subsequently, a reverse centrifugation at 1,000 × g for 2 min was performed to recover the EVs. Once recovered, the EVs were resuspended in PBS and centrifuged again to remove any remaining contaminants, followed by another reverse centrifugation to recover the EVs and transfer them to a clean tube. The final volume obtained for each sample was approximately 1.2 mL. The samples were then subjected to SEC.

2.7. Size Exclusion Chromatography (SEC)

The protocol provided by the manufacturer IZON was followed. Prior to loading the column, the samples were processed to have the same volume of 1.2 mL, of which 200 µL were labeled with 1 µL of the fluorophore 3,3'-Dioctadecyloxacarbocyanine Perchlorate (DiOC18) and incubated for 30 min at 37 °C to locate fractions containing EVs among the 26 collected fractions.

The columns were prepared with PBS by performing two washes. First, 1 mL of the sample was passed through the column, and 26 fractions of 0.7 mL each were collected. Then, the DiOC-labeled sample was diluted with PBS to complete a volume of 1 mL and passed through the column to obtain another 26 fractions of 0.7 mL each.

Subsequently, the fractions were placed into a Costar 3603 96-well plate, and two 100 µL aliquots of each fraction were pipetted for reading. The pre-established method "Method_GLA_SEC" was used for measurement, and the fractions with the highest signal were selected.

2.8. Characterization of EVs

2.8.1. WB

The same procedure described in previous sections for SDS-PAGE and Western blot of soluble GLAs was followed for GLAs loaded within EVs.

2.8.2. Nanoparticle Tracking Analysis NTA

The vesicle samples were resuspended in phosphate-buffered saline (PBS) previously filtered through a 0.22 µm filter. The concentration was adjusted by performing serial dilutions with PBS. Data acquisition was carried out by capturing consecutive 60 s videos at a constant temperature. The data were analyzed using NTA software.

2.8.3. Transmission Electron Microscopy

Negative staining was performed using 2% phosphotungstic acid (PTA) over 200-mesh copper grids coated with formvar and carbon following established procedures. Prior staining 5 µL of EV (approx. XXX EVs) was gently applied to the working surface of each grid without forming bubbles and incubated for 20 min. Grids were visualized using a transmission electron microscopy (TEM) JEOL JEM 1010 80kV at the facilities of the University of Barcelona (UB).

2.8.4. Enzymatic Activity

The enzymatic activity of α-galactosidase A (GLA) was assessed using a fluorometric assay adapted from the original method described by Desnick et al., with modifications by Mayes et al., and applied in previous studies from our research group. This assay is based on the hydrolysis of the non-fluorescent substrate 4-methylumbelliferyl-α-D-galactopyranoside (4-MUG), which is converted by active GLA into the fluorescent product 4-methylumbelliferone (4-MU). The reaction was carried out in an acetate buffer (0.01 M acetic acid, 0.01 M acetate, pH 4.5), using 10 mM 4-MUG (Sigma-Aldrich) as substrate. A typical reaction mixture consisted of 100 µL of substrate and 25 µL of sample, incubated with constant agitation (GLS Aqua 12 Plus, 25 rpm) at 37 °C for 1 hour. The reaction was terminated by adding 1.25 mL of glycine buffer (0.2 M, pH 10.4), and the released 4-MU fluorescence was measured using a microplate reader (FLx800™, Biotek™) with excitation at 365 nm and emission at 450 nm. To reduce variability, two dilutions of each sample were analyzed in duplicate. A calibration curve was prepared with commercial 4-MU standards

(5–500 ng/mL in glycine buffer), enabling the conversion of fluorescence units into 4-MU concentration. Enzymatic activity results were normalized based on reaction time and protein content.

Micro BCA Assay

Protein concentration was determined by Micro BCA assay following the manufacturer's instructions (Micro BCA™ Protein Assay Kit, Thermo Scientific).
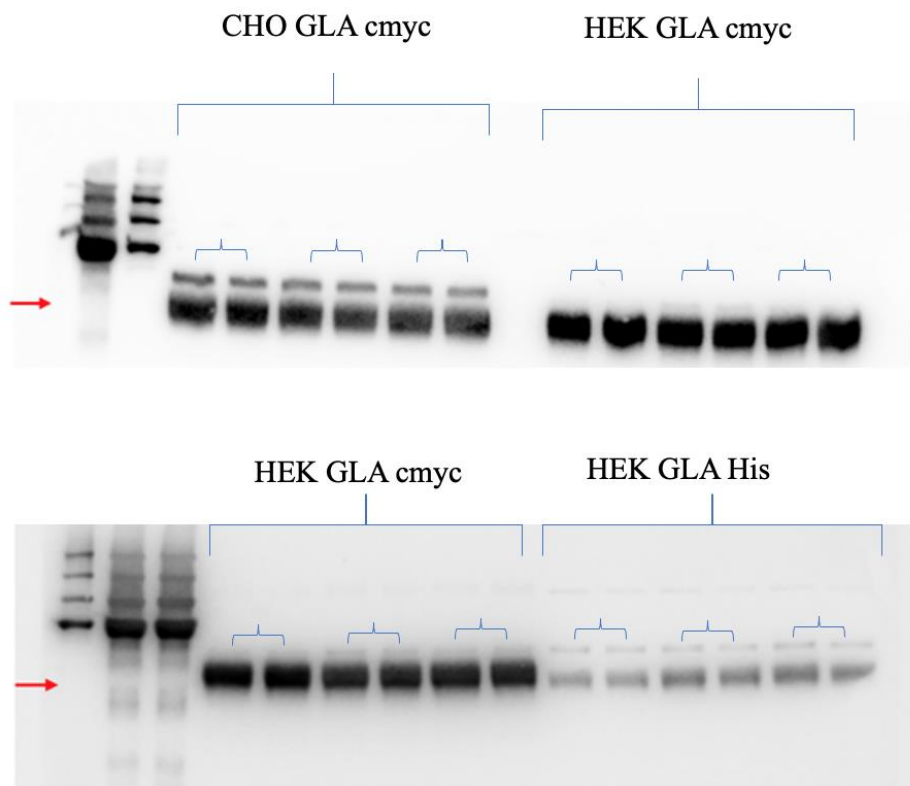
3. Results

3.1. Protein production

Figure 4. Western blot analysis of α-galactosidase A (GLA) expression in HEK and CHO cells. a) Intra and extracellular expression of stable CHO clones and transiently transfected HEK cells with Cmyc tagged constructs. b) Intra and extracellular expression of transiently transfected HEK cells with Cmyc tagged GLA and HIS tagged GLA constructs.
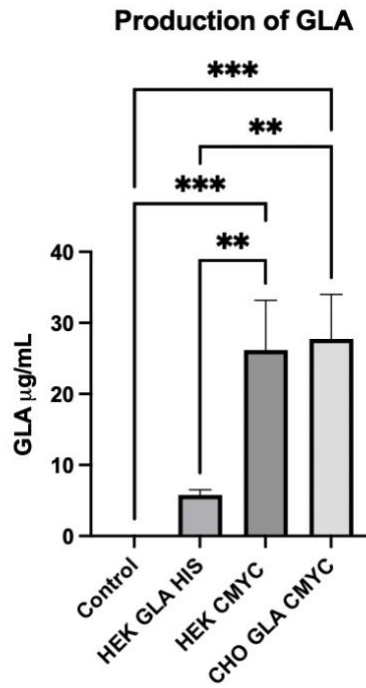
Figure 5. The two GLA cmyc constructs are present at similar levels, significantly higher than HEK GLA his.

Table1. Production of protein in cells HEK and CHO

	Replicate	Supernatant volume mL	Initial cell number	Final cell number	Supernatant µg/ml	Soluble protein µg/ml
HEK GLA HIS	n1 BTF	125	$1.06 \cdot 10^6$	$1.6 \cdot 10^6$	0	0
	n2 TFF	60	$1.06 \cdot 10^6$	$1.5 \cdot 10^6$	5.8	3.1
	n3 TFF	60	$1.06 \cdot 10^6$	$1.5 \cdot 10^6$	5.1	3.4
	n4 BTF	250	$1.06 \cdot 10^6$	$1.6 \cdot 10^6$	6.5	3.6
HEK GLA CMYC	n1 BTF	125	$1.06 \cdot 10^6$	$1.5 \cdot 10^6$	0	0
	n2 TFF	60	$1.06 \cdot 10^6$	$1.6 \cdot 10^6$	18.5	18.4
	n3 TFF	60	$1.06 \cdot 10^6$	$1.5 \cdot 10^6$	27.8	22.3
	n4 BTF	250	$1.06 \cdot 10^6$	$1.5 \cdot 10^6$	32.2	24.7
CHO GLA CMYC	n1 BTF	125	$1x10 \cdot 10^6$	$6.8 \cdot 10^6$	0	0
	n2 TFF	60	$1x10 \cdot 10^6$	$6.5 \cdot 10^6$	21.5	17.8
	n3 TFF	60	$1x10 \cdot 10^6$	$5.6 \cdot 10^6$	27.6	18.1
	n4 BTF	300	$1x10 \cdot 10^6$	$6.5 \cdot 10^6$	34.1	31.9
CONTROL	n1 BTF	125	$1.06 \cdot 10^6$	$1.5 \cdot 10^6$	N/A	N/A
	n2 TFF	60	$1.06 \cdot 10^6$	$1.6 \cdot 10^6$	N/A	N/A
	n3 TFF	60	$1.06 \cdot 10^6$	$1.5 \cdot 10^6$	N/A	N/A
	n4 BTF	150	$1.06 \cdot 10^6$	$1.5 \cdot 10^6$	N/A	N/A

compare the yield and quality of EVs produced by HEK293 and CHO cell lines expressing α-GLA. CHO GLA cMyc and HEK GLA cMyc constructs demonstrated significantly higher expression yields compared to the HEK GLA His construct. Although no statistically significant difference was observed between CHO GLA cMyc and HEK GLA cMyc, the presence of the cMyc tag appears to enhance protein stability and half-life. The smaller size of the cMyc-tagged construct may facilitate sustained functional expression, enabling optimal production. These findings indicate that, although CHO cells are classically optimized for recombinant protein production, HEK293 cells can achieve comparable yields when equipped with the cMyc tag and cultured under optimal conditions.
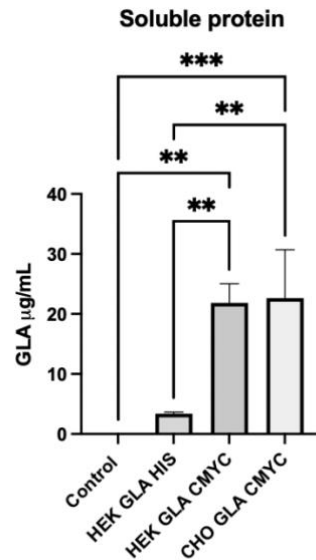

Figure 6. MicroBCA quantification of His-trap purified protein. Protein is properly purified, and the same trend observed in Figure 5 is maintained. The two GLA cmyc constructs are present at similar levels, significantly higher than HEK GLA his.
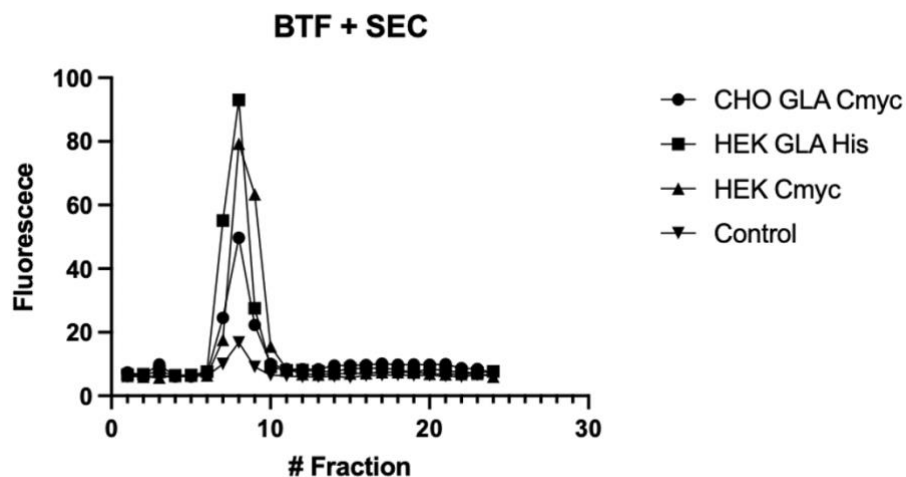
3.2. Purification of EVs

Figure 7. Size Exclusion Chromatography (SEC) od EVs sample obtained by benchtop filtration (BTF). It is observed that the fraction with the highest signal are 7,8 and 9 for all three type of samples
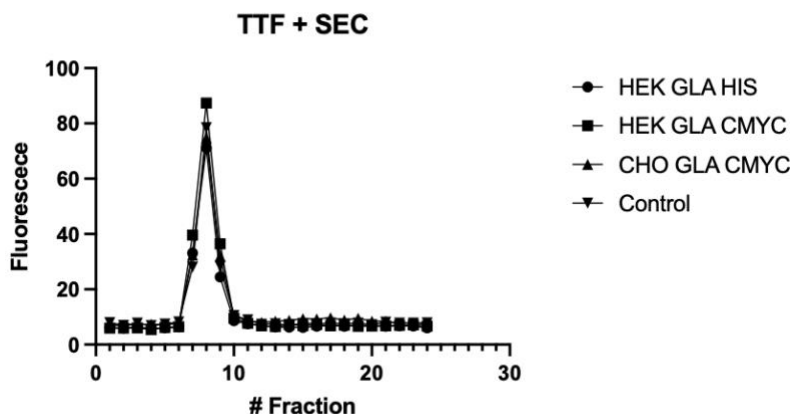

Figure 8. Size Exclusion Chromatography (SEC) of EVs sample obtained by tangential flow filtration (TFF). It is observed that the fractions with the highest signal corresponding to EVs are fractions 6, 7, 8, 9, and 10. HIS and CHO samples show a higher signal compared to the control and cMyc.
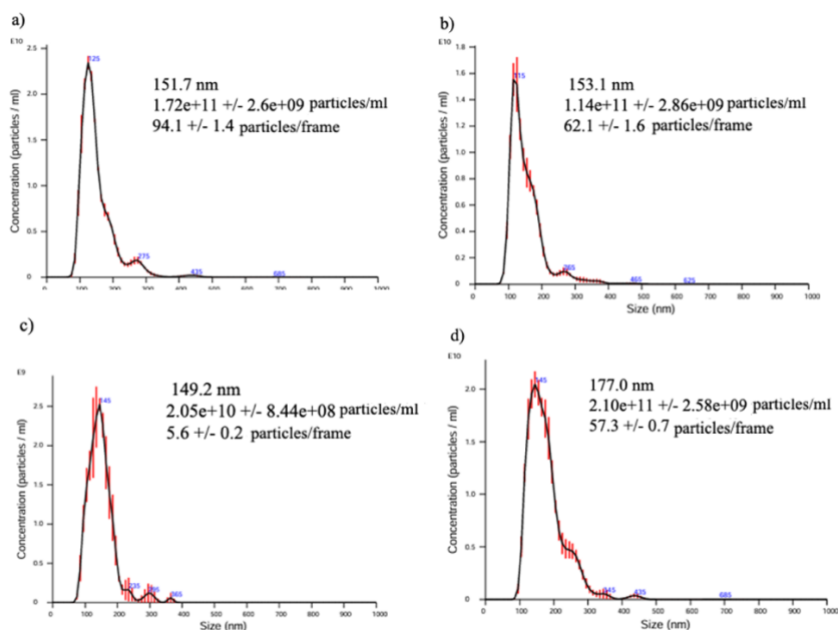
Figure 9. Nanoparticle Tracking Analysis (NTA) sample obtained by benchtop filtration (BTF). It is observed size, concentration (particles/mL), and particles per frame. a) HIS, b) CMYC, c) CHO y d) Control
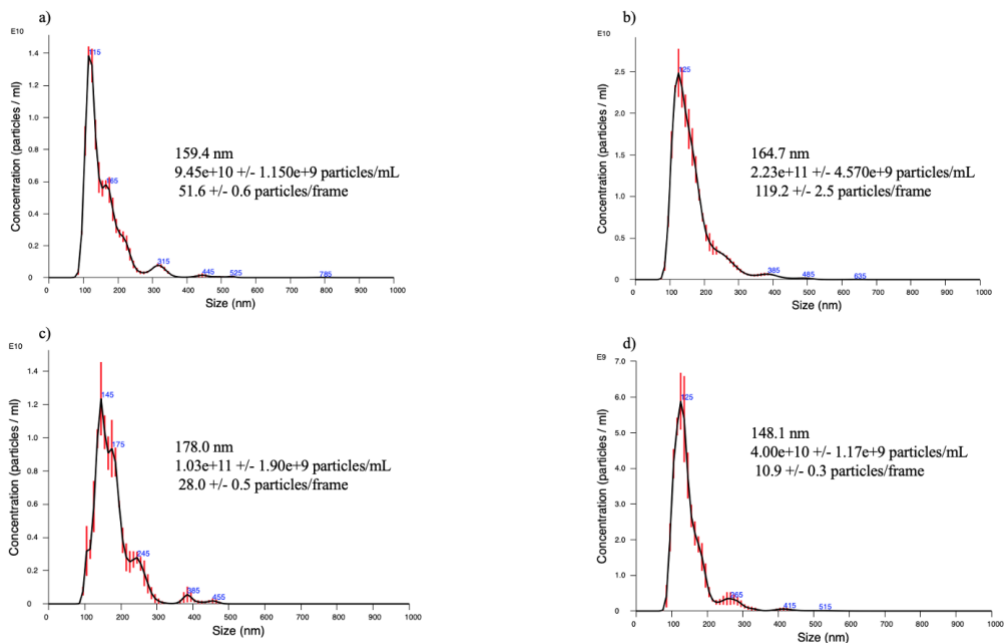

Figure 10. Nanoparticle Tracking Analysis (NTA) sample obtained by TFF. It is observed size, concentration (particles/mL), and particles per frame. a) HIS, b) CMYC, c) CHO y d) Control

The impact of different isolation methods on the purity, integrity, and enzymatic activity of EVs loaded with GLA. Tangential Flow Filtration (TFF) consistently outperformed Bottom-Through Filtration (BTF) in EV yield. This improved recovery is associated with greater enzymatic activity and vesicle integrity, likely due to TFF's parallel flow mechanism, which applies reduced shear stress and minimizes membrane fouling. These results underscore the critical impact of the purification method on both the quantity and quality of functional EVs
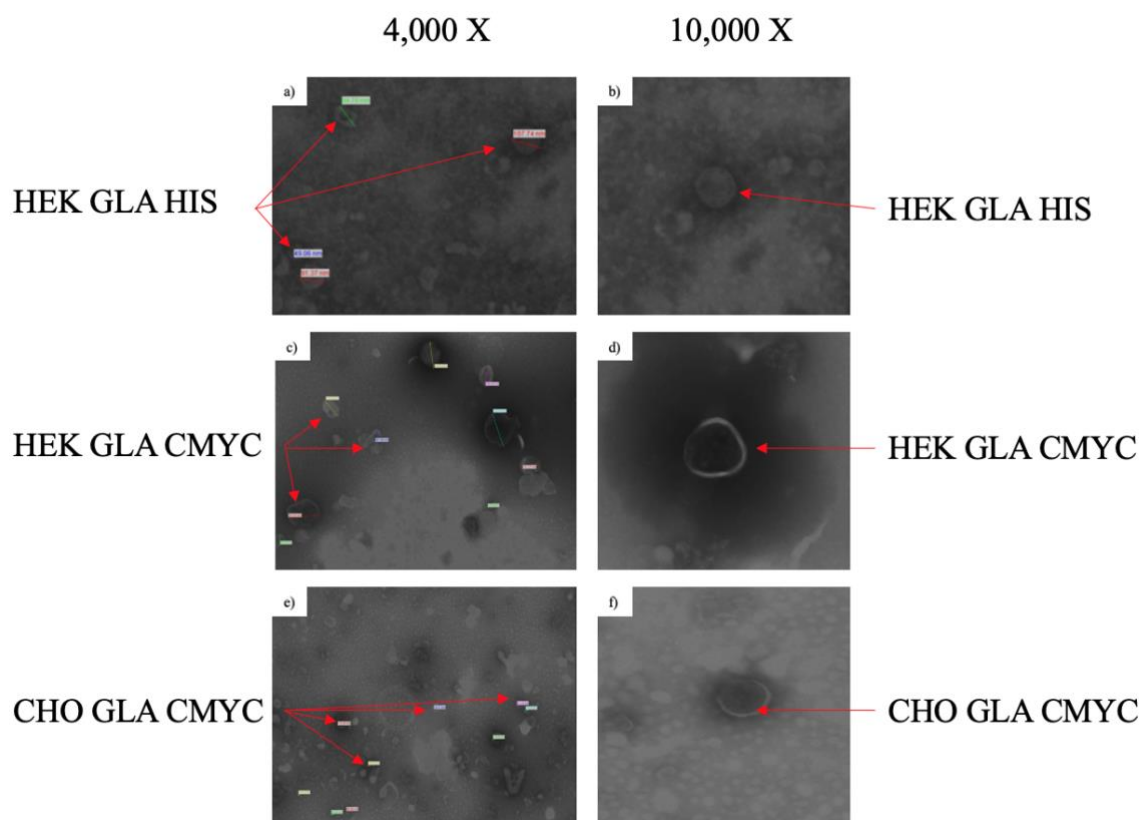

Figure 11. Transmission Electron Microscopy (TEM) EVs obtained at different magnifications.a) EVs from CHO n4 at 4000x, b) EVs from CHO n4 at 10000x, c) EVs from CHO-Cmyc n4 at 4000x, d) EVs from CHO-Cmyc n4 at 10000x, e) EVs from CHO-His n4 at 4000x, f) EVs from CHO-His n4 at 10000x. All micrographs show spherical structures surrounded by a lipid bilayer, which is characteristic of EVs.

Table 2. Evs production and enzymatic activity

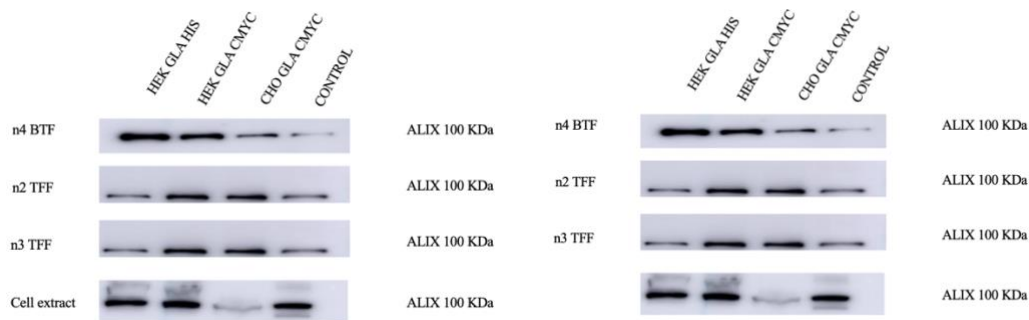| Type of EV	EV GLAHIS HEK		EV CmycHIS HEK		EV CmycHIS CHO		EV Control	
Isolation method	**n1BF + SEC**	**n2TFF + SEC**	**n1BF + SEC**	**n2 TFF + SEC**	**n1 BF + SEC**	**n2 TFF + SEC**	**n1 BF + SEC**	**n2 TFF + SEC**
Size (nm)	219.4	151.7	200.7	153.1	215.8	149.2	200.8	177
Particles/mL	$3.59 \cdot 10^9 \mp 4.38 \cdot 10^8$	$1.72 \cdot 10^{11} \mp 2.6 \cdot 10^9$	$1.80 \cdot 10^8 \mp 2.99 \cdot 10^8$	$1.14 \cdot 10^{11} \mp 2.86 \cdot 10^9$	$7.27 \cdot 10^9 \mp 2.05 \cdot 10^8$	$2.05 \cdot 10^{10} \mp 8.44 \cdot 10^8$	$3.94 \cdot 10^9 \mp 4.06 \cdot 10^8$	$2.10 \cdot 10^{11} \mp 2.58 \cdot 10^9$
Particles/frame	2.0 ∓ 0.2	94.1 ∓ 1.4	1.0 ∓ 0.1	62.1 ∓ 1.6	39.7 ∓ 1.1	5.6 ∓ 0.2	53.8 ∓ 0.1	57.3 ∓ 0.7
GLA concentration ug GLA/L	2.4	2.7	114	302.3	189	459.7	0	0
Enzimatic activity 4MU (ngmL)	859.4	1,173.2	710.1	1,995.5	8494.6	8,503.9	0	0
Enzimatic activity 4MU (ngmL)	873.8	1,205.6	688.3	1,924.8	8,230.7	8,375.1	0	0
Enzimatic activity 4MU (ngmL)	894.2	1,139.7	732.5	2,051.2	8,610.3	8,488.6	0	0
SD	14.4	33.0	31.3	89.4	268.4	80.3	0	0

Figure 12. Characterization of EV biomarkers by Western blot.. a) ALIX 100 KDa b) GLA 50 KDa methodologies
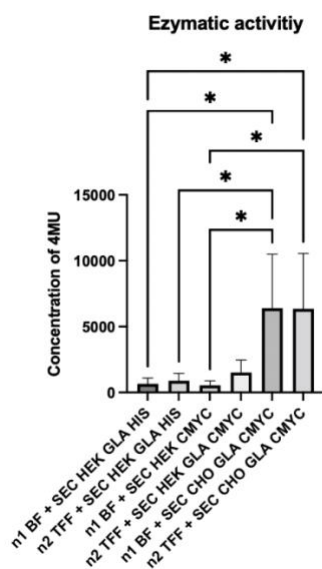

Figure 13. Enzymatic activity BTF vs TFF

Optimal production and purification conditions to maximize the efficacy of EVs as a delivery system for Fabry disease therapy. Prolonged exposure to imidazole during metal-affinity purification was found to impair GLA enzymatic activity, highlighting the importance of downstream processing steps, particularly buffer exchange or dialysis, to preserve enzyme function. When pairing CHO GLA cMyc constructs with TFF purification, the resulting EVs exhibit a favorable profile in terms of yield, structural integrity, and functional enzymatic

activity—positioning this combination as a robust, scalable, and promising platform for the development of EV-based enzyme replacement therapy (ERT) for Fabry disease.

3.3. Discussion

The first phase of this project focused on GLA production. Two approaches were employed for the expression of α-galactosidase A (GLA): transient transfection in HEK293 cells to generate GLA-His and GLA CMYC, and a stable clone in CHO cells to produce GLA CMYC. As shown in Figure 6, the CHO-cMyc system achieved markedly higher yields of GLAcompared to the others, particularly outperforming GLA HIS from HEK293. This aligns with literature indicating that CHO-based systems can reach recombinant protein yields of 3–10 g/L, a benchmark recognized for production efficiency and reproducibility in the biopharmaceutical industry. In contrast, yields from transient expression in HEK293 systems typically fall within the range of 100–600 mg/L. The enhanced expression observed in the HEK CMYC system—relative to HEK HIS—could be attributed to the presence of the CMYC epitope, as demonstrated by Mikelis et al. (2005) in their study of the kinase ERK3. They reported that incorporation of a C-terminal CMYC tag extended the protein's half-life compared to the untagged version, suggesting the tag mitigates protein degradation and thus prolongs detection.

Meanwhile, the relatively low yield from HEK-GLA-His may stem from the properties of the HIS-tag. Woestenenk et al. (2004) noted that HIS-tags positioned at either the N or C-terminus can reduce solubility and promote aggregation or precipitation—issues particularly problematic in transient expression systems where culture volume is limited. Additionally, Williams et al. (2018) observed that HIS-tags can adversely affect protein function, stability, and conformational dynamics—challenges that are especially critical for GLA, given that its proper conformation is essential for secretion and stability.

Upon successful production of GLA in these various systems, the next phase involved purification of both the enzyme and extracellular vesicles (EVs). Soluble GLA was purified using His SpinTrap columns based on metal-affinity chromatography, with imidazole

employed for elution. However, this step resulted in a loss of enzymatic activity, consistent with findings by Kutyshenko et al. (2018), who reported that imidazole can induce autoinactivation or accelerated degradation of proteins. Therefore, a protocol incorporating His SpinTrap purification followed by dialysis was established to remove imidazole, which interferes with spectrophotometric measurements and enzymatic assays. This strategy is supported by Ramans et al. (2022), who emphasized that eliminating residual compounds such as imidazole and transitioning to stabilizing buffers is effective in preserving protein conformation and functionality.

Once GLA production was achieved in the predetermined cell lines, the second phase of the project commenced: the purification of EVs containing GLA. Two purification strategies were tested: bottom-through filtration (BTF) and tangential flow filtration (TFF). As shown in Table 2, TFF exhibited a higher yield compared to BTF, a finding supported by Tian et al. (2018), who reported that although BTF has been traditionally used to concentrate and isolate EVs, it presents several limitations—especially when processing small volumes—due to the potential loss of material and collapse of vesicular membranes. In contrast, TFF allows parallel flow along the filter surface, minimizing the pressure exerted on vesicles and reducing membrane clogging, which enhances recovery and integrity. The enzymatic activity (EA) of GLA does not appear to be compromised during the TFF (Tangential Flow Filtration) process, despite the enzyme's prolonged exposure to room temperature during diafiltration. On the contrary, EA levels observed in EVs purified via TFF were higher compared to those obtained through BTF (Bottom-Through Filtration). This suggests that the TFF method not only maintains the structural integrity of the vesicles but may also better preserve the enzymatic functionality of the encapsulated GLA, potentially due to the gentler processing conditions and more efficient removal of interfering solutes.

Similarly, Visan et al. (2022) compared BTF and TFF for the isolation of EVs derived from various human and murine cell lines, followed by SEC purification. While both methods are applicable, TFF proved to be a more reliable and robust technique in terms of yield, processing time, cost-effectiveness, and scalability. Busatto et al. (2018) further emphasized that TFF is a more efficient and less aggressive method, concentrating EVs with comparable physicochemical properties, higher recovery, and reduced levels of soluble macromolecules and aggregates. Moreover, it provides greater batch-to-batch consistency.

Regarding EV yield, CHO GLA-cMyc cells produced a higher number of vesicles, which correlates with existing evidence showing that CHO cells are extensively optimized for protein secretion. A comparative transcriptomic analysis revealed that HEK cells exhibit elevated activity in the unfolded protein response (UPR) and ER-associated degradation (ERAD) pathways, whereas CHO cells show enhanced capacity for correct protein folding, leading to properly assembled proteins. This is supported by Kalluri and LeBleu (2020), who state that highly secretory cells tend to release more EVs as a complementary mechanism for transporting proteins and lipids. Another important factor is that CHO cells can achieve higher cell densities with superior viability, maintaining cellular integrity under stress and reducing cell death. Jeppesen et al. (2019) also reported that CHO cells exhibit differential expression of genes associated with EV biogenesis, such as components of the endosomal sorting complex required for transport (ESCRT) and Rab GTPases, which are more active under specific conditions, thereby promoting increased production of exosomes and microvesicles.

In terms of enzymatic activity, the results demonstrated that EVs from CHO GLA-cMyc purified by TFF displayed superior enzymatic function compared to the other groups. This may be attributed to the higher GLA cargo within the EVs and to the preservation of vesicular integrity during the TFF process. This aligns with findings from Walsh (2014) and Fischer et al. (2015), who described that GLA, as a lysosomal enzyme, requires precise folding, post-translational modifications, and proper intracellular trafficking for optimal activity—characteristics well-documented in CHO expression systems. Furthermore, the cMyc tag, due to its small size and structural flexibility, appears to minimally interfere with enzymatic functionality, particularly when placed at the C-terminus, as shown by Hengen (1995) and Li et al. (2020).

4. Conclusions

- In the first part of the master's project, recombinant protein production was achieved using different constructs, with CHO GLA cMyc and HEK GLA cMyc yielding the best results.

- For protein purification, it is essential to remove all components that may interfere with protein stability, such as imidazole. In this case, dialysis proved to be a simple and effective method.

- For extracellular vesicle (EV) purification, TFF showed better efficiency compared to BTF, likely due to the gentler nature of the method and the temperature conditions under which the samples are processed.

- Enzymatic activity depends not only on the amount of GLA produced but also on its proper folding, stability, and integrity to perform its function. Therefore, considering both production and purification, using CHO cells with a cMyc tag and purifying via TFF appears to be a strong candidate for enzyme replacement therapy.

5. References

Abasolo, I., Seras-Franzoso, J., Moltó-Abad, M., Díaz-Riascos, V., Corchero, J. L., Pintos-Morell, G., & Schwartz, S. (2021). Nanotechnology-based approaches for treating lysosomal storage disorders, a focus on Fabry disease. *WIREs Nanomedicine and Nanobiotechnology*, *13*(3), Article 3. https://doi.org/10.1002/wnan.1684

Abreu, R. C. de, Fernandes, H., Martins, P. A. da C., Sahoo, S., Emanueli, C., & Ferreira, L. (2020). Native and engineered extracellular vesicles for cardiovascular therapeutics. *Nature Reviews. Cardiology*, *17*(11), Article 11. https://doi.org/10.1038/s41569-020-0389-5

Alipourfetrati, S., Saeed, A., Norris, J. M., Sheckley, F., & Rastogi, A. (2015). A Review of Current and Future Treatment Strategies for Fabry Disease: A Model for Treating Lysosomal Storage Diseases. *Journal of Pharmacology and Clinical Toxicology*, *3*(3), Article 3. https://doi.org/10.47739/1051

Azevedo, O., Gago, M. F., Miltenberger-Miltenyi, G., Sousa, N., & Cunha, D. (2020). Fabry Disease Therapy: State-of-the-Art and Current Challenges. *International Journal of Molecular Sciences*, *22*(1), Article 1. https://doi.org/10.3390/ijms22010206

Bozzuto, G., & Molinari, A. (2015). Liposomes as nanomedical devices. *International Journal of Nanomedicine*, *10*, 975-999. https://doi.org/10.2147/IJN.S68861

Cooper, J. M., Wiklander, P. B. O., Nordin, J. Z., Al-Shawi, R., Wood, M. J., Vithlani, M., Schapira, A. H. V., Simons, J. P., El-Andaloussi, S., & Alvarez-Erviti, L. (2014). Systemic exosomal siRNA delivery reduced alpha-synuclein aggregates in brains of transgenic mice. *Movement Disorders: Official Journal of the Movement Disorder Society*, *29*(12), Article 12. https://doi.org/10.1002/mds.25978

Coutinho, M. F., Santos, J. I., & Alves, S. (2016). Less Is More: Substrate Reduction Therapy for Lysosomal Storage Disorders. *International Journal of Molecular Sciences*, *17*(7), Article 7. https://doi.org/10.3390/ijms17071065

Del Grosso, A., Parlanti, G., Mezzena, R., & Cecchini, M. (2022). Current treatment options and novel nanotechnology-driven enzyme replacement strategies for lysosomal storage disorders. *Advanced Drug Delivery Reviews*, *188*, 114464. https://doi.org/10.1016/j.addr.2022.114464

Doyle, L. M., & Wang, M. Z. (2019). Overview of Extracellular Vesicles, Their Origin, Composition, Purpose, and Methods for Exosome Isolation and Analysis. *Cells*, *8*(7), Article 7. https://doi.org/10.3390/cells8070727

Ferreira, C. R., & Gahl, W. A. (2017). Lysosomal storage diseases. *Translational Science of Rare Diseases*, *2*(1-2), Article 1-2. https://doi.org/10.3233/TRD-160005

Glassman, P. M., & Muzykantov, V. R. (2019). Pharmacokinetic and Pharmacodynamic Properties of Drug Delivery Systems. *The Journal of Pharmacology and Experimental Therapeutics*, *370*(3), Article 3. https://doi.org/10.1124/jpet.119.257113

Guérard, N., Morand, O., & Dingemanse, J. (2017). Lucerastat, an iminosugar with potential as substrate reduction therapy for glycolipid storage disorders: Safety, tolerability, and pharmacokinetics in healthy subjects. *Orphanet Journal of Rare Diseases*, *12*(1), Article 1. https://doi.org/10.1186/s13023-017-0565-9

Gupta, D., Wiklander, O. P. B., Görgens, A., Conceição, M., Corso, G., Liang, X., Seow, Y., Balusu, S., Feldin, U., Bostancioglu, B., Jawad, R., Mamand, D. R., Lee, Y. X. F., Hean, J., Mäger, I., Roberts, T. C., Gustafsson, M., Mohammad, D. K., Sork, H., … El-Andaloussi, S. (2021). Amelioration of systemic inflammation via the display of two different decoy protein receptors on extracellular vesicles. *Nature Biomedical Engineering*, *5*(9), Article 9. https://doi.org/10.1038/s41551-021-00792-z

Hughes, D., Gonzalez, D., Maegawa, G., Bernat, J. A., Holida, M., Giraldo, P., Atta, M. G., Chertkoff, R., Alon, S., Almon, E. B., Rocco, R., & Goker-Alpan, O. (2023). Long-term safety and efficacy of pegunigalsidase alfa: A multicenter 6-year study in adult patients with Fabry disease. *Genetics in Medicine: Official Journal of the American College of Medical Genetics*, *25*(12), Article 12. https://doi.org/10.1016/j.gim.2023.100968

Juszkiewicz, K., Sikorski, A. F., & Czogalla, A. (2020). Building Blocks to Design Liposomal Delivery Systems. *International Journal of Molecular Sciences*, *21*(24), Article 24. https://doi.org/10.3390/ijms21249559

Kimiz-Gebologlu, I., & Oncel, S. S. (2022). Exosomes: Large-scale production, isolation, drug loading efficiency, and biodistribution and uptake. *Journal of Controlled Release*, *347*, 533-543. https://doi.org/10.1016/j.jconrel.2022.05.027

Lenders, M., Stappers, F., & Brand, E. (2020). In Vitro and In Vivo Amenability to Migalastat in Fabry Disease. *Molecular Therapy. Methods & Clinical Development*, *19*, 24-34. https://doi.org/10.1016/j.omtm.2020.08.012

Leone, D. A., Rees, A. J., & Kain, R. (2018). Dendritic cells and routing cargo into exosomes. *Immunology and Cell Biology*. https://doi.org/10.1111/imcb.12170

Lu, B., Ku, J., Flojo, R., Olson, C., Bengford, D., & Marriott, G. (2022). Exosome- and extracellular vesicle-based approaches for the treatment of lysosomal storage disorders. *Advanced Drug Delivery Reviews*, *188*, 114465. https://doi.org/10.1016/j.addr.2022.114465

Miller, J. J., Kanack, A. J., & Dahms, N. M. (2020). Progress in the understanding and treatment of Fabry disease. *Biochimica Et Biophysica Acta. General Subjects*, *1864*(1), Article 1. https://doi.org/10.1016/j.bbagen.2019.129437

Morimoto, H., Ito, Y., Yoden, E., Horie, M., Tanaka, N., Komurasaki, Y., Yamamoto, R., Mihara, K., Minami, K., & Hirato, T. (2018). Non-clinical evaluation of JR-051 as a biosimilar to agalsidase beta for the treatment of Fabry disease. *Molecular Genetics and Metabolism*, *125*(1-2), Article 1-2. https://doi.org/10.1016/j.ymgme.2018.07.009

Nakamura, K., Kawashima, S., Tozawa, H., Yamaoka, M., Yamamoto, T., Tanaka, N., Yamamoto, R., Okuyama, T., & Eto, Y. (2020). Pharmacokinetics and pharmacodynamics of JR-051, a biosimilar of agalsidase beta, in healthy adults and patients with Fabry disease: Phase I and II/III clinical studies. *Molecular Genetics and Metabolism*, *130*(3), Article 3. https://doi.org/10.1016/j.ymgme.2020.04.003

Rombach, S. M., Aerts, J. M. F. G., Poorthuis, B. J. H. M., Groener, J. E. M., Donker-Koopman, W., Hendriks, E., Mirzaian, M., Kuiper, S., Wijburg, F. A., Hollak, C. E. M., & Linthorst, G. E. (2012). Long-term effect of antibodies against infused alpha-galactosidase A in Fabry disease on plasma and urinary (lyso)Gb3 reduction and treatment outcome. *PloS One*, *7*(10), Article 10. https://doi.org/10.1371/journal.pone.0047805

Sahoo, S., Adamiak, M., Mathiyalagan, P., Kenneweg, F., Kafert-Kasting, S., & Thum, T. (2021). Therapeutic and Diagnostic Translation of Extracellular Vesicles in Cardiovascular Diseases. *Circulation*, *143*(14), Article 14. https://doi.org/10.1161/CIRCULATIONAHA.120.049254

Seras-Franzoso, J., Díaz-Riascos, Z. V., Corchero, J. L., González, P., García-Aranda, N., Mandaña, M., Riera, R., Boullosa, A., Mancilla, S., Grayston, A., Moltó-Abad, M., Garcia-Fruitós, E., Mendoza, R., Pintos-Morell, G., Albertazzi, L., Rosell, A., Casas, J., Villaverde, A., Schwartz, S., & Abasolo, I. (2021). Extracellular vesicles from recombinant cell factories improve the activity and efficacy of enzymes defective in lysosomal storage disorders. *Journal of Extracellular Vesicles*, *10*(5), Article 5. https://doi.org/10.1002/jev2.12058

Ståhl, A.-L., Johansson, K., Mossberg, M., Kahn, R., & Karpman, D. (2019). Exosomes and microvesicles in normal physiology, pathophysiology, and renal diseases. *Pediatric Nephrology (Berlin, Germany)*, *34*(1), Article 1. https://doi.org/10.1007/s00467-017-3816-z

Torchilin, V. P. (2005). Recent advances with liposomes as pharmaceutical carriers. *Nature Reviews. Drug Discovery*, *4*(2), Article 2. https://doi.org/10.1038/nrd1632

Wallace, E. L., Goker-Alpan, O., Wilcox, W. R., Holida, M., Bernat, J., Longo, N., Linhart, A., Hughes, D. A., Hopkin, R. J., Tøndel, C., Langeveld, M., Giraldo, P., Pisani, A., Germain, D. P., Mehta, A., Deegan, P. B., Molnar, M. J., Ortiz, D., Jovanovic, A., … Warnock, D. G. (2024). Head-to-head trial of pegunigalsidase alfa versus agalsidase beta in patients with Fabry disease and deteriorating renal function: Results from the 2-year randomised phase III BALANCE study. *Journal of Medical Genetics*, *61*(6), Article 6. https://doi.org/10.1136/jmg-2023-109445

West, M., Nicholls, K., Mehta, A., Clarke, J. T. R., Steiner, R., Beck, M., Barshop, B. A., Rhead, W., Mensah, R., Ries, M., & Schiffmann, R. (2009). Agalsidase alfa and kidney dysfunction in Fabry disease. *Journal of the American Society of Nephrology: JASN*, *20*(5), Article 5. https://doi.org/10.1681/ASN.2008080870

Wilczewska, A. Z., Niemirowicz, K., Markiewicz, K. H., & Car, H. (2012). Nanoparticles as drug delivery systems. *Pharmacological Reports: PR*, *64*(5), Article 5. https://doi.org/10.1016/s1734-1140(12)70901-5

Yetisgin, A. A., Cetinel, S., Zuvin, M., Kosar, A., & Kutlu, O. (2020). Therapeutic Nanoparticles and Their Targeted Delivery Applications. *Molecules (Basel, Switzerland)*, *25*(9), Article 9. https://doi.org/10.3390/molecules25092193

Zeb, A., Rana, I., Choi, H.-I., Lee, C.-H., Baek, S.-W., Lim, C.-W., Khan, N., Arif, S. T., Sahar, N. us, Alvi, A. M., Shah, F. A., Din, F. ud, Bae, O.-N., Park, J.-S., & Kim, J.-K. (2020). Potential and Applications of Nanocarriers for Efficient Delivery of Biopharmaceuticals. *Pharmaceutics*, *12*(12), Article 12. https://doi.org/10.3390/pharmaceutics12121184